Surface enhanced Raman spectroscopy as a probe for local modification of carbon films

A. Ilie,* C. Durkan, W. I. Milne, and M. E. Welland
Engineering Department, Cambridge University, Cambridge CB2 1PZ, United Kingdom
(Received July 13, 2001; revised manuscript received 25 February 2002; published 25 July 2002)

The possibility of achieving nanometer-scale sensitivity in a surface-enhanced Raman (SERS) experiment while using larger-sized probes (0.1–1 μm) is investigated. The application targeted is carbon film transformation under high-energy beam irradiation, and, primarily, the transformation of amorphous carbon into nanocrystalline graphite. The carbon film covers nanometer-size Ag particles which enhance the signal from zones of material adjacent to them. This geometry gives access to the film/substrate interface, and in this way it complements scanning near-field techniques which have similar spatial sensitivity but are mainly surface sensitive. The SERS effect has been studied as a function of the Ag nanoparticle size, carbon film thickness, and excitation wavelength. A selective enhancement of the Raman cross section of the *D* band of amorphous carbons was observed. The dielectric properties of the carbon film, when used as an overlayer, strongly affect the SERS enhancement, so that changes in the dielectric function upon irradiation can be used to produce local enhancement contrast, and to establish an identification procedure for material transformation.

DOI: 10.1103/PhysRevB.66.045412 PACS number(s): 78.30.Ly, 81.05.Uw, 81.07.−b, 81.40.Tv

I. INTRODUCTION

There is increasing interest in producing carbon materials with a structure that varies on the nanometer scale. These will take advantage of the unique property of carbon that, solely by varying the type of bonding, very different local properties can be obtained, ranging from diamond to graphitelike or nanotubelike. The applications of these materials can be various, such as large area electron-field emitters,[1–6] or, at the other end of the spectrum, as antifuses[7] and nanodevices in nanotechnology.

Various deposition techniques allow the direct manufacture of thin films with mixed sp^2 and sp^3 phases.[1–6] However, the spatial distribution of the two phases is random in these cases, while for the applications mentioned above it is desirable to be able to controllably induce a nanostructure of a specific type and at predetermined locations. One way to achieve this goal is to use high-energy ion or electron beams to locally transform a given matrix. In this way, graphitic regions can be formed in a diamondlike matrix,[8] or fullerenes in amorphous carbon or graphitic materials,[9] or, conversely, graphitic materials, such as fullerenes, can be transformed into diamond.[10]

Probing the extent of a local transformation is not always easy. Ideally, we would like to use a technique which (i) has a nanometer scale sensitivity, (ii) can be tuned to probe various depths in the film down to the film-substrate interface, and (iii) provides structural information. Atomic force microscopy (AFM) can reveal a contrast between irradiated and nonirradiated zones based on their different conductivities; nevertheless, due to the small size of the probed area, this technique is restricted to materials or regions with rather high conductivity ($>10^{-5}\ \Omega^{-1}\,\mathrm{cm}^{-1}$), and, in addition, it does not provide direct structural information. Energy-loss-spectroscopy (EELS) is a powerful structural characterization technique at the nanometer scale;[11] however, the information obtained is global, integrated over the film bulk and interfaces. Cross-sectional EELS can alleviate this problem,[12] but it is very difficult to apply to the study of nanometer scale regions embedded in an matrix.

Here we focus on the surface enhanced Raman (SERS) technique, which can potentially satisfy the requirements listed above. Indeed, Raman spectroscopy is the technique of choice for identifying bonding in various carbon systems,[13–18] while its surface-enhanced variant has been used for the detection of low-dimensionality objects, such as single-wall nanotubes[19] and single molecules,[20,21] and for the study of interfacial phenomena and ultrathin films.[22–24] Usually, nm-scale Raman information is obtained using scanning near-field optical microscope (SNOM) techniques, and to date the highest spatial resolution reported was about 100–150 nm with aperture-based SNOMs[25,26] and about 50 nm when using an apertureless microscope.[27]

We investigated an alternative way to detect nm size active areas in carbon films of tens of nm thickness, while still using larger-sized Raman probes of 0.1–1 μm. This utilizes the selective enhancement of the signal I^* from the zone of interest (e.g. modified by irradiation in our target application) when this is adjacent to Ag nanostructures, so that I^* rises above the nonenhanced background I given by the remaining probed area (unmodified). When expressed in terms of the respective surfaces, this condition leads to $S^*R>S$, where S^* and S are the areas of the enhanced and nonenhanced regions, respectively, S^*+S is the total probed area, and R is the enhancement factor for region S^*. For S^*+S in the range 10^4-10^6 nm^2 (as for 0.1–1-μm diameter probes), an enhancement factor $R\approx 10^3-10^4$ is sufficient to allow the signal from a region S^* with a diameter as low as 30 nm to largely dominate the overall signal. We were interested mainly in the configuration with the carbon film grown on top of the Ag nanostructures, in order to probe the effectiveness of the transformation down to the substrate, as required above; this configuration gives complementary information to that from SNOM techniques, which are sensitive mainly to the top surface.

We explored the feasibility of this technique primarily in conjunction with tetrahedral amorphous carbon (ta-C), the form of amorphous carbon with the highest sp^3 bonding

content (~85%).[28] ta-C is interesting since, due to the presence of some sp^2 bonding, it has a higher propensity for transformation into a graphitic phase through irradiation or thermal annealing than diamond,[8] though retaining many diamondlike properties. While no irradiation was performed in this study, our aim was to check the prerequisites to perform such a SERS experiment: whether there is sufficient enhancement for selective nm-scale sensitivity, how the Raman spectra change relative to the well-known bulk spectra, and whether there are additional dependencies such as on the carbon overlayer thickness.

We found that the magnitude of the SERS effect varies with the ta-C overlayer thickness, and with different dependencies when changing the excitation wavelength. For a micron-size probe the intensity of the SERS signal increased by about 10^3-10^4 relative to the normal Raman signal when increasing the wavelength to the infrared. This is already sufficient enhancement to meet our purpose of selective detection using larger size probes. The complex behavior with the overlayer thickness and excitation wavelength, was discussed by considering two possible competitive effects: (i) tuning into the SERS resonance of the carbon-coated Ag nanostructures, an effect related to the dielectric function of the carbon film; and (ii) optical interference accompanying Raman scattering as the carbon film thickness is comparable to the excitation wavelength. The SERS effect is found to be highly sensitive to the interfacial layer of the ta-C film, which is more sp^2 rich, but it also extends into the film's bulk. This high sensitivity is also accompanied by a larger dispersion with energy of the $I(D)/I(G)$ parameter, the ratio of the intensities of the Raman D and G bands, than for normal Raman scattering in any bulk carbon material. This is the first report of a selective enhancement of the Raman D band in amorphous carbons through a surface-enhanced effect.

We also discuss the sensitivity of the SERS effect to changes in the dielectric properties of the overlayer, as occur in an irradiation experiment. Therefore, amorphous diamondlike and graphitic regions will show a clear enhancement contrast, despite having features in the same spectral range. This allowed us to set a simple procedure for assessing when the local transformation from a diamondlike phase toward a graphitic phase takes place. The SERS technique described here can work particularly well for transformations in which the final phase has a low imaginary part of the dielectric constant and Raman features in a different spectral region than the initial phase, e.g. amorphous carbon into onions, or fullerenes into diamond.

II. SERS AND SURFACE PLASMONS IN Ag NANOSTRUCTURES

The SERS effect induced by small noble metal particles appears to be of complex origin. The main volume of data generated in the last two decades points, essentially, to an electromagnetic enhancement with a near-field upper value of about 10^7-10^8, which is due to the excitation of surface plasmon resonances,[29] covering the spectral range from visible to near-UV. Only recently, made possible by the development of near-field scanning techniques, have some notable disagreements with this approach been observed. Accordingly, very peculiar, individual ''hot'' particles have been identified,[20,21] which are responsible for a huge *local* enhancement, up to 10^{14}, so that single molecules could be detected. Recent calculations based on the numerical resolution of the Maxwell's equations showed that the sharp angles of particles with irregular shape can generate a near-field enhancement locally in excess of 10^{12}, which can be correlated with polarization charge distributions.[30] Effects other than electromagnetic, such as chemical or nonlinear optical effects (e.g., hyper-Raman scattering),[21] were also invoked in the case of the hot particles. Collective systems, such as fractal colloidal systems, were also found to give a local-field enhancement in excess of 10^{10},[31–33] but with the peculiarity that the resonances can now reach the microwave range, i.e., far away from the classical plasmon resonances.[31]

Here the Raman signal is averaged over a larger (μm size) area, and comes from well-formed, continuous overlayers, so that it is difficult to distinguish local effects on rare ''hot'' particles, whether present or not. In addition, the morphology of our Ag films is rather periodic, and nonfractal (see Sec. III). Therefore, we will explain our data only in the framework of the classical surface plasmon formalism. This has given a good description of photon emission induced by a scanning tunneling microscope on the same type of Ag films.[34] As the Ag nanostructures lie beneath the Raman-active layer, our main interest is to relate the magnitude and spectral dependence of the observed SERS effect to the properties of the overlayer.

A surface plasmon is a collective oscillation mode of conduction electrons which occurs at the surface of solids under external electromagnetic excitation. Localized (bound) plasmon fields can be excited if the surface is broken into small structures, such as gratings, spheroidal particles, or just via mere roughness. The electric field of the plasmon reaches a resonance for a certain frequency ω_{pl}. In the case of an isolated, small spheroidal metal particle, the plasmon field is dipolar, and related to the excitation field E_0 by a factor depending on the ratio of the dielectric constants of both metal and environment, ε_m and ε, respectively, and on the depolarization factor A of the particle:

$$E=\frac{\varepsilon_m(\omega)/\varepsilon(\omega)}{1+[\varepsilon_m(\omega)/\varepsilon(\omega)-1]A}E_0=\beta(\omega)E_0. \qquad (1)$$

Relation (1) describes the field just outside the particle's surface. E will be greatly enhanced, i.e., having a resonance, if the excitation is at that ω_{pl} for which

$$\mathrm{Re}[\varepsilon_m(\omega)/\varepsilon(\omega)]=1-1/A. \qquad (2)$$

For a sphere $A=\frac{1}{3}$, so that the resonance condition becomes $\mathrm{Re}[\varepsilon_m(\omega)/\varepsilon(\omega)]=-2$.

ω_{pl} of a small Ag sphere in air is about 3.4 eV (near the UV). One gets an idea about how the plasmon resonance is modified by overlayers from relation (2). This shows that by increasing $\mathrm{Re}(\varepsilon)=\varepsilon_1$ of the embedding environment (which can be seen as an infinite overlayer), ω_{pl} shifts to ~3.2 eV in water ($\varepsilon_1=1.77$), to 3 eV in cyclohexane ($\varepsilon_1=2.04$), and to

2 eV (red) in an hypothetical nonabsorbing medium with $\varepsilon_1 \sim 6-7$, as that of ta-C [Fig. 1(a)]. Because here the carbon overlayers vary from several to hundreds of nm, one has to investigate how overlayers of finite thickness affect $\omega_{\rm pl}$. This will be discussed in Sec. V.

SERS is based on the enhancement of the Raman intensity of the vibrating group through two effects: first, the electric field felt by the Raman dipole is enhanced due to the excitation of the plasmon resonance in the adjacent Ag particle; second, the field of the Raman dipole itself, which is at the frequency $(\omega-\omega_v)$ for the Stokes process, can cause a further enhancement of the Ag particle field if $(\omega-\omega_v)$ is in the width of the plasmon resonance; ω_v is the vibrational frequency. Therefore, the enhanced Raman intensity I will depend on the product of two enhancement factors, one at the excitation frequency ω and another at $(\omega-\omega_v)$, so that it is proportional to the square of the induced dipole moment:

$$I \sim |\beta(\omega)\beta(\omega-\omega_v)|^2. \tag{3}$$

If ω_v is small compared to ω, and if, moreover, the resonance is broad, then, from Eqs. (1) and (3), $I \sim |E(\omega)|^4$. The SERS local enhancement factor G is then

$$G = |E|^4/|E_0|^4. \tag{4}$$

Relation (4) is valid for visible SERS on amorphous and disordered carbons, since they have small vibrational frequencies ω_v, of the order 0.2 eV.

For applications involving relatively thick ($\sim$ tens of nm) films, as here, one needs to know the distance which can be probed by the SERS effect, i.e., the spatial extension of the plasmon electric field r_p. For a dipolar resonance, E is at a maximum just outside the Ag nanosphere, and then decreases with the distance r in the medium of dielectric constant ε as

$$|E(r)| = (4\pi/3)^{1/2}|2cr^{-3}-d|, \tag{5}$$

where c and d are constants depending on the dielectric functions of Ag and the carbon overlayer. G thus varies rapidly with the distance from the nanosphere surface, as $1/r^{12}$. Here we define r_p as the distance at which E decays to E_0. To obtain the actual SERS intensity I for an overlayer of thickness t, one has thus to integrate G over t:

$$I \sim \int_0^{r_p} |E(r)|^4 dr + |E_0|^4 (t-r_p) \approx \int_0^{r_p} |E(r)|^4 dr. \tag{6}$$

For high enhancement factors, $|E_0|^4(t-r_p)$ can be neglected in Eq. (6), so that the direct dependence of I on t disappears. In contrast, the nonenhanced Raman intensity I_0 increases with t because the volume available for scattering increases. We can then have an approximate expression for the integral SERS enhancement factor $R = I/I_0$: the measured quantity

$$R = I/I_0 \approx \frac{\int_0^{rp} |E(r)|^4/|E_0(r)|^4 dr}{t}. \tag{7}$$

There are two factors which can affect simple relation (7). One is related to optical absorption in the carbon film; this can decrease the intensity incident on the narrow region r_p located near the film-substrate interface, and, subsequently, also the Raman scattered signal originating from r_p on its way back toward the film surface. However, since the optical gap of this ta-C is about 3.5 eV,[35] the absorption coefficient α is very low ($<10^2$ cm^{-1}) in the film bulk for excitation energies in the visible range, as used here. Higher absorption can occur in the more sp^2 interfacial layer of ta-C (see Secs. III and IV). However, this effect should be rather weak as this layer is only a few nm thick. The second factor affecting Eq. (7) is related to interference, which can occur in both normal and surface-enhanced Raman scattering,[36–38] and introduce modulations dependent on t and the excitation wavelength λ. As quantified below in Sec. IV, this effect is important for specular surfaces and interfaces, but decreases strongly with increasing film roughness.

It is important to note that relation (2) is valid only in the limit of the quasistatic theory (Rayleigh), i.e., for Ag particles of size a small enough relative to the excitation wavelength λ [$a < 0.05\lambda/\sqrt{\mathrm{Re}(\varepsilon)}$ (Ref. 39)] so that they seem embedded in a static field, and a nonretarded potential can be used. The embedding medium is considered as infinite. This condition limits a to about 10–15 nm when ta-C is used as the overlayer, and for excitation energies in the 1.6–2.4-eV range as used here. For larger size particles, retardation effects become important, and therefore a full electrodynamic formalism (Lorentz-Mie) has to be applied.[40] In this case, though the dipolar contribution to the plasmon electromagnetic field is still dominant, multipolar terms cannot be neglected.[39,40] Furthermore, the dipolar resonance is damped, broadened, and redshifted, while the multipolar resonances are sharp and at high energies.[39]

To increase the SERS effect above the single small sphere values given by the formalism above, one can increase the aspect ratio from sphere to spheroid (the ''lightning rod'' effect), and pack the structures closely so that the resonances couple. Recent calculations of collective electromagnetic effects in strongly coupled, periodic spheroidal features,[41] as on a rough surface, showed that a surface *averaged* Raman enhancement as large as 10^5-10^6 is possible for appropriate ''close packing,'' and this despite larger (above the quasistatic limit) features. Figure 1(b) shows such a situation, when semicylinders are packed so that they touch each other ($d=2r$, where d is the distance between the centers of the semicylinders while r is their radius). Moreover, the *local* enhancement can be even larger, up to 10^7-10^8, at the crevices between features.[41] As expected, the resonance is broad and redshifted; however, the very strong coupling between features makes it more stable in frequency and magnitude than in the case of isolated Mie scattering centers. Therefore, size-related retardation effects only shift the resonance from 3.4 to about 2.6–2.8 eV in this case,[41] as opposed to about 2 eV for isolated features of the same size.[39] Note that for a nonfractal surface (as in Ref. 41), with periodic boundary conditions, the more collective nature of the plasmon oscillations reduces the enhancement below the local values in

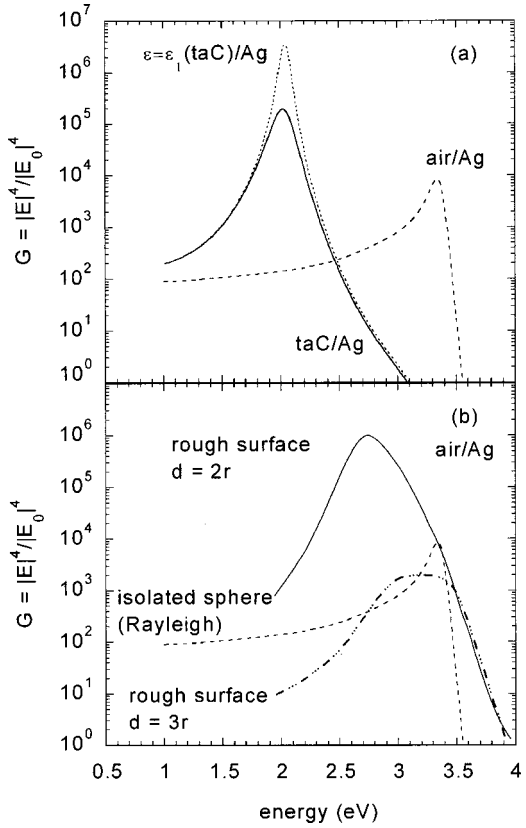

FIG. 1. (a) SERS enhancement and position of the plasmon resonance for a small (in the Rayleigh limit), isolated Ag sphere in air (dashed line), in an infinite hypothetical medium with $\varepsilon=7$ as ε_1 of bulk ta-C (dotted line), and in a medium with $\varepsilon=7+i0.6$ as that of ta-C (plain line). (b) Comparison between the SERS resonance of Ag spheres placed in air, in the Rayleigh limit (~18 nm) and in the Lorentz-Mie formalism (for 30-nm spheres). Optimal packing ($d=2r$) gives higher spatially averaged enhancement than nonoptimal packing ($d>2r$) (Ref. 41).

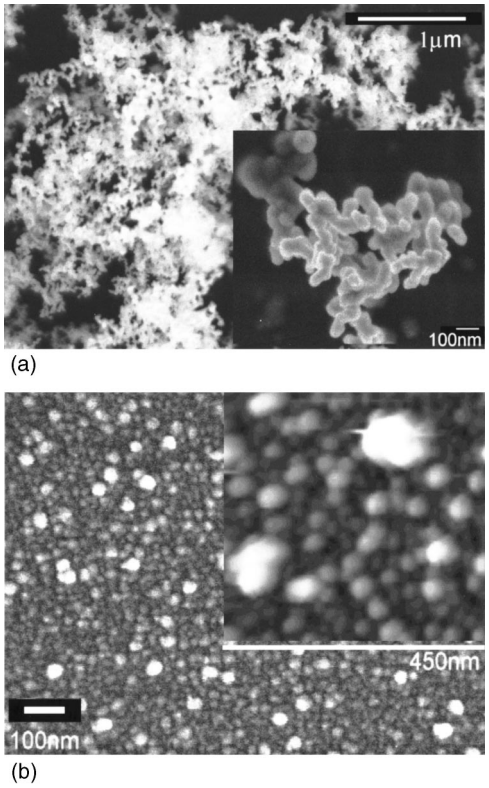

FIG. 2. Self-assembled Ag nanostructures obtained by thermal evaporation in (a) Ar atmosphere, and (b) He atmosphere. The images are obtained with FEG-SEM, except the inset from (b) which is an AFM scan. In (b), the AFM scan has a better definition then the FEG-SEM image; nevertheless the particles sizes are affected by the convolution with the tip, especially for the larger particles.

fractal systems, where enhancements in excess to 10^{10} can be obtained as the excitations remain more localized.[31]

III. FILM FABRICATION AND MORPHOLOGY

The Ag nanostructures used in this study were produced by two self-assembly methods: (i) thermal evaporation in an inert gas atmosphere, and (ii) slow etching of continuous Ag films in vapors of nitric acid. These methods are easy to apply on a larger scale, but difficult to implement to define nm size enhancement regions as required in a final experiment, when only the signal from a specific zone has to be enhanced. Nevertheless, the self-assembled nanostructures allow us to assess the magnitude of the SERS effect achievable with carbon films and the factors which control it. Well-defined periodic structures, with sizes down to about 20 nm (to decrease retardation effects), and controlled positioning are being produced with *e*-beam lithography, and the results will be presented elsewhere.

The presence of an inert atmosphere during Ag evaporation causes the Ag atoms to lose energy (to ''cool'') and to cluster together before they reach the substrate.[42] The morphology of the Ag films produced in this way was varied by changing the type and pressure p of the inert gas, the distance between the source and the substrate d, and the evaporation rate v. Ag structures were also produced by etching continuous layers in vapors of nitric acid. This technique is convenient and can give a uniform substrate coverage, but the surface topography is difficult to control and the resulting structures are coarse and irregular.

Figure 2(a) shows a scanning electron micrograph (FEG-SEM) of the topography of Ag films produced in Ar at $p=1$ Torr, $d\sim10$ cm, and $v\sim10$ Å/sec. These films have a porous aspect, and a three-dimensional topology which confers them a high roughness. Higher magnification reveals building blocks as small as 50 nm, connected in a rather random way. Fast Fourier transform (FFT), radially averaged, of this topography shows uniform contributions in a very large frequency range, which is characteristic for fractal films. Figure 2(b) shows FEG-SEM and AFM (inset) topographies of films produced in He at $p=0.7$ Torr, $d\sim5$ cm, and at a much lower evaporation rate $v\sim0.2$ Å/sec. These conditions were set to decrease the cluster size and to increase their uniformity and coverage. These films are clearly different from those from Fig. 2(a), and three categories of sizes of spheroidal clusters can be distinguished: (i) a basic structure of clusters of about 17 ± 5-nm diameter, densely packed, on top of which there are (ii) isolated clusters of

about 40 ± 5 nm, with a surface density of about $70/\mu m^2$, and (iii) larger, isolated clusters of about 65 ± 5 nm and density $4/\mu m^2$. Note that only the smaller clusters reach the electrostatic limit set in Sec. II for ta-C overlayers. The cluster sizes were obtained by comparing AFM and FEG-SEM images. Radially averaged FFT reveals important contributions only in a limited frequency range, corresponding to the three size categories, as opposed to a fractal topography.

ta-C was deposited from a cathodic arc with an *S*-bend filter[43] at a floating potential, i.e. from C^+ ions at 20 eV, in several configurations: (i) on Si substrates, (ii) on flat (SERS inactive) Ag films, (iii) on the nanostructured Ag films described above, and (iv) with the nanostructured Ag films on top. The ta-C thickness was varied from 10 to ~120 nm, covering a range interesting for irradiation experiments, and estimated through ellipsometry and the deposition rate. ta-C is usually characterized by a high sp^3 bonding content, around 85%. On the other hand, it has been found that the growth mechanism of ta-C also leads to several-nm-thick interfacial and surface layers which are about 30% less dense, and, thus, more graphitic than the film bulk;[44,45] carbon was found to mix with the substrate atoms in the first monolayers.[12] In addition, films prepared using a single-bend filtered cathodic arc were found to have a multilayered structure (and, thus, variable density) even in the bulk;[44] The ta-C films produced here with the *S*-bend arc have a much more homogeneous structure despite the low ion energy used, with a bulk layer of uniform density and 87% sp^3 content, and very thin (1–2-nm thick) interface and surface layers.[44] Metallic substrates were found to promote increased sp^2 bonding in the interfacial layer of various amorphous carbons when compared to Si substrates.[46] A Raman analysis of our ta-C films deposited on flat Ag films (see Sec. IV) showed that the interface with Ag suffers only a moderate modification compared to the interface with Si, which could be consistent with sp^2 promotion and increased interfacial disorder. The nanostructured Ag films from Fig. 2(b) have similar topographies with or without ta-C overlayers (confirmed by both AFM and SEM), indicating that carbon layers in our thickness range uniformly cover the Ag clusters, and that there is no cluster coalescence during ta-C deposition.

IV. SERS OF CARBON THIN FILMS

We acquired unpolarized Raman spectra in the backscattering geometry using three excitation wavelengths, of 514.5 nm (green), 633 nm (red) and 785 nm (near-infrared), in order to determine the position of the plasmon resonance. Large beam as well as confocal experimental setups were used, varying the probe size from 10 μm to about 1 μm, respectively, to obtain information about spatial uniformity and surface averaging of the enhancement; as expected, more nonuniform values were obtained with the 1-μm probe.

In carbon systems containing sp^2 bonding, the visible Raman features are entirely due to the sp^2 phase, even if the sp^2 content is low, such as in ta-C (~15%). This is due to two reasons. (i) The Raman-scattering cross section of the sp^2 phase is about 50–230 times higher than that of the sp^3 phase[47] due to the longer-range polarizability modulation of the π bonds.[48] These values are for 514.5-nm excitation. (ii) Visible Raman is resonant in materials with an sp^2 phase.[49–51] This comes from the fact that the sp^2 phase determines the optical gap by introducing electronic states over the entire range from IR to UV, so that Raman scattering takes place with a real photon absorption on the appropriate electronic levels.

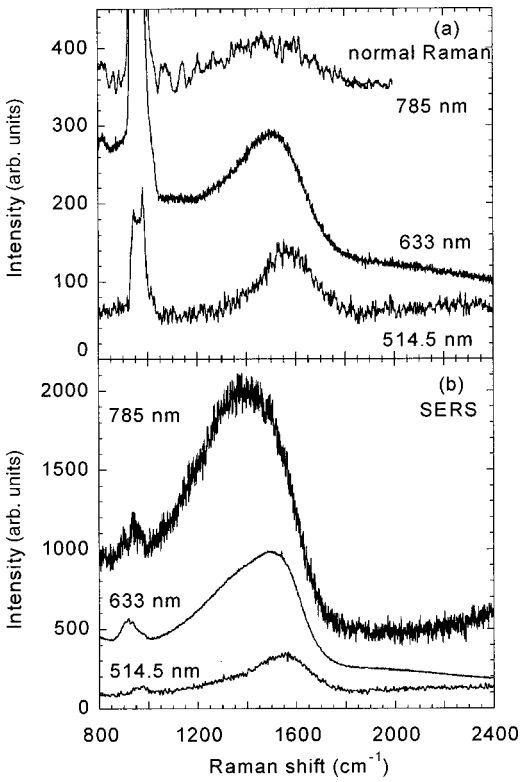

FIG. 3. Unpolarized (a) normal Raman and (b) SERS spectra of ta-C for various excitation wavelengths. The near-infrared (785 nm) activity of ta-C in normal Raman is extremely weak compared with the two other wavelengths, requiring long acquisition times.

A green Raman spectrum of bulk ta-C on non-SERS Si substrates is shown in Fig. 3(a). This consists of a broad *G* peak centered around 1560–1580 cm^{-1}, which is attributed to the same in-plane bond-stretching vibrations of sp^2 C-C bonds (the E_{2g^2} mode), as in graphite.[13] In an amorphous matrix, however, disorder relaxes the $\vec{q}\approx0$ phonon quasiselection rule valid in a crystal, allowing all the phonons in the Brillouin zone, and not only those around the Γ point (as in graphite), to participate in scattering.[52] This then allows contributions from sp^2 sites with bond angle disorder,[53] and explains the large width of the *G* peak in ta-C compared with that in HOPG or nanocrystalline graphite. The shape of the *G* peak can be fitted by a Breit-Wigner-Fano function.[54]

Another feature present in the Raman spectra of carbons with disordered sp^2 phase is the *D* peak around 1360 cm^{-1}. In nanocrystalline graphite, its increase in intensity relative to the *G* peak, I_D/I_G, has been related to the decrease in size of the ordered graphitic crystallites.[13] Conversely, in systems where an sp^3 phase is still present, as in amorphous or nanostructured carbons, it has been observed that the increase in

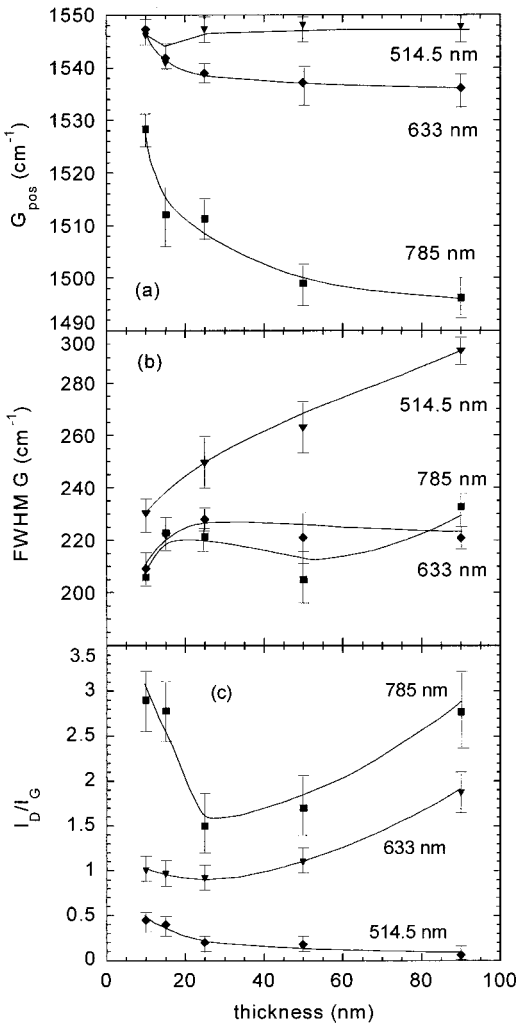

FIG. 4. Raman parameters after deconvolution of the SERS spectra into *D* and *G* peaks; Lorentzian and Breit-Wigner-Fano line shapes were used, respectively.

I_D/I_G correlates with ordering into aromatic rings and increase in size of the sp^2 phase inside the sp^3 matrix.[15,16,55] The origin of the *D* peak remains controversial, and explanations such as a resonant or double-resonant effect[56,57] or an A_{1g} breathing mode of aromatic ring clusters have been proposed.[16] The spectra of bulk ta-C do not show a *D* peak for any excitation energy, suggesting that there is no organization into aromatic rings of the sp^2 phase. However, for the thinnest ta-C film (<10 nm) on Si the I_D/I_G parameter is nonzero and the *G* peak is broader, indicating a noticeable contribution to the Raman scattering from the interface and subsurface regions, so that bulk properties are not entirely dominant. These effects become slightly larger for equivalently thin ta-C films deposited on flat (SERS inactive) Ag substrates.

The ta-C spectra on SERS active substrates show a broad feature around 1300–1700 cm^{-1}, with a *D* peak shoulder [Fig. 3(b)] at all thicknesses. No other narrow bands[58] or lines showing strong fluctuations from site to site[59] were detected in our experiments. The results of deconvolution of our spectra into *D* and *G* peaks are shown in Figs. 4(a)–4(c). A Lorentzian was used for the fit of the *D* peak; the error bars are due to different choices of baseline, and nonhomogenenity of the Ag films. As the *D* peak is not related to bulk ta-C, it can only be due to the interfacial layer of ta-C in contact with the Ag structures, which experiences the highest enhancement. A *D* peak indicative of more graphitic interfaces has also been observed in a combination of SERS and interference Raman spectroscopy, when a diamondlike carbon layer was sandwiched between Al and Ag layers;[37] similar to our case, the bulk film did not present a *D* peak.[37] Nevertheless, the interface for our films appears to be closer to the diamond like phase than that in Ref. 37 (at 514.5 nm, our spectra present a less pronounced *D* peak when compared to the spectra from Ref. 37). An extrinsic contribution to the *D* peak may also come from a buildup of the amorphous carbon contamination due to residual hydrocarbon cracking by a gas ionization source (such as ion gauges).[60] We checked this and found that in our vacuum conditions (about 10^{-7} mbar) a weak *a*-C carbon signal can be obtained from Si substrates covered only with Ag. Various substrate cleaning procedures involving acids or organic solvents did not significantly change these results. On the other hand, thick Ag layers did not give any carbon signature, proving that the signal does not come from Ag itself, but from monolayers of *a*-C building up on the substrate prior to Ag deposition.

The variation of the *G* peak parameters with increasing ta-C thickness is consistent with an increasing sensitivity of the SERS effect to the film's bulk. The *G* peak position [Fig. 4(a)] at low thickness disperses with energy as in amorphous carbons with more ordered sp^2 phases, while for thicker films there is much higher dispersion, characteristic of a more disordered material, such as ta-C (Ref. 51); for ta-C there is a strong *G* peak dispersion from 1570 nm to below 1480 nm, for the same wavelength range. The *G* peak's full width at half maximum (FWHM) is shown in Fig. 4(b). For thin films, the FWHM is about 200–240 cm^{-1}, and there is no significant dispersion with energy; this behavior is characteristic of carbon systems with moderate disorder.[51] The FWHM then increases slightly with thickness, indicative of a transition from a more graphitic to a more disordered material such as ta-C.[51] This therefore shows that the SERS effect also probes the bulk ta-C. At 514.5-nm (2.4-eV) excitation, an increase with the thickness of the FWHM is accentuated, tending toward that of ta-C ($\sim$300 cm^{-1}), but we attribute part of this to the less uniform absorption of light at this energy.

The *D* peak position only gives information about the sp^2 phase in the interfacial layer (as a *D* peak is not present in bulk ta-C). A 1340–1370-cm^{-1} value is rather typical of amorphous carbons annealed at moderate temperatures, indicating more order of the sp^2 phase than, for example, in as-deposited *a*-C:H, where the *D* peak is located around 1270 cm^{-1}.[51] I_D/I_G [Fig. 4(c)] has the most interesting behavior of all the Raman parameters, as for any thickness it has *higher dispersion with energy than any bulk carbon material*. In normal Raman scattering, the dispersion of the *D* peak in materials with a distribution of sp^2 clusters has been attributed to resonant Raman scattering, indicating that by

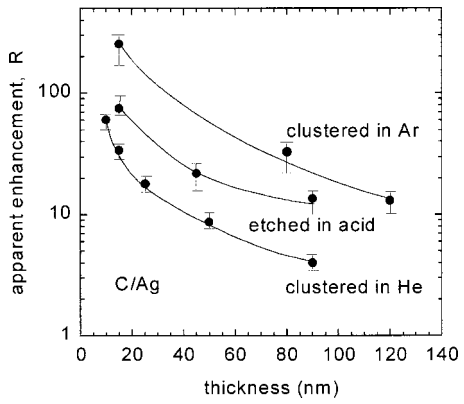

FIG. 5. Apparent enhancement factor ($R=I/I_0$) as a function of ta-C overlayer thickness, for various Ag nanostructures. Green wavelength (514.5 nm) has been used.

decreasing the energy, clusters of larger size, and thus smaller gap[61] are selected and probed.[50,51] This means that I_D/I_G is expected to disperse more in materials with more ordered and significant sp^2 phase. However, the range spanned in normal Raman scattering[51] is significantly less than that obtained here with SERS. We attribute this strong dispersion and sensitivity of the SERS effect to the *D* band to a preferential enhancement of the Raman cross section through an enhanced coupling of the sp^2 phase with the electromagnetic field. As the *D* peak is related to the clustering of the sp^2 phase into aromatic rings, these are expected to show anisotropy in the polarizability. The electromagnetic coupling would then increase if the directions of maximum polarizability and the electric field of the incident radiation coincide.[29] Preferential enhancement and broadening of some vibrational modes relative to the others were also observed in the case of C_{60} and copperphthalocyanine (CuPc), an organic molecule, and attributed to preferential orientation of the aromatic rings and electric field gradients over the molecules.[38]

Figure 5 shows the dependence of the integral SERS factor $R=I/I_0$ (the ratio of the intensity of the enhanced and nonenhanced Raman peaks) on ta-C thickness for 514.5-nm excitation, and for the various Ag nanostructures described in Sec. III. A higher enhancement was obtained on the irregular structures shown in Fig. 2(a). We attribute this to the higher roughness and non-homogeneity of these films compared to the more ordered films from Fig. 2(b). On the other hand, *R* was found to decrease with increasing *t* with similar rates for all types of films, despite different *R* values. Almost the same thickness dependence was also found upon varying the excitation wavelength λ down to near-infrared (Fig. 6). As the nonenhanced intensity I_0 introduces a $1/t$ dependence on *R* (see Sec. II), this common behavior upon thickness regardless of the wavelength and film topography suggests that any variation of the enhanced intensity *I* with *t* is dominated by that in $1/t$ of I_0, as in formula (7). Figure 6 also shows that increasing the excitation wavelength to near-infrared increases *R*, which means that the plasmon resonance is strongly redshifted. *R* values between 10^3-10^4 were obtained for 785 nm excitation [Fig. 6(b)].

Figure 7(a) shows the dependence of the enhanced intensity *I* on the film thickness for various λ's. For green excitation *I* increases with *t*, to reach a maximum around 40 nm, then decreases. The same (*I*-*t*) behavior is obtained in red excitation, with the shape of the curve slightly shifted and less variation. However, in the near-infrared region maximum disappears and the beginning of a plateau is obtained for the highest thicknesses. This shows that the variable thickness of the ta-C overlayer causes a complex wavelength dependence of the SERS effect, the origin of which will be discussed below in Sec. V.

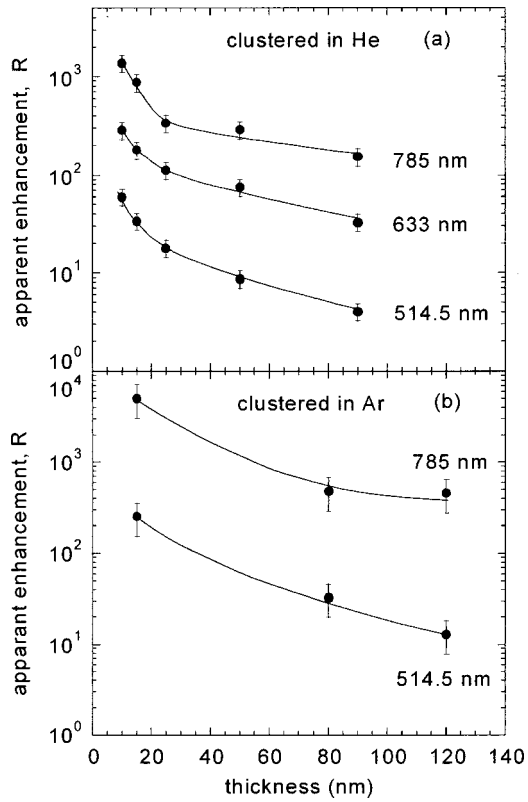

FIG. 6. Apparent enhancement factor ($R=I/I_0$) as a function of the ta-C overlayer thickness, for different excitation wavelengths; Ag clusters were produced in (a) He and (b) Ar atmosphere. The error bars are due to the nonhomogeneneity of the Ag films, and obtained by comparing ten spectra from different locations on the sample.

Figure 7(b) compares the situations when ta-C is on top or underneath the Ag nanostructures. Due to the limited electric-field range r_p associated with the plasmon excitation [see relation (6)], the configuration with ta-C on top of Ag (C/Ag) allows us to probe regions of ta-C close to the substrate, while when the ta-C is underneath the Ag (Ag/C) the subsurface region is probed. While C/Ag gives the resonant behavior described above, the Ag/C configuration gives a constant value of *I* above ~20 nm. This shows that (i) the resonant behavior for C/Ag from Fig. 7(a) is due to the ta-C layer and not to Ag, and (ii) r_p in ta-C is less than about 20–30 nm. In addition, the analysis of the Raman parameters of the SERS spectra corresponding to the two configurations C/Ag and Ag/C indicates that the resulting bottom and top interfaces are similar, so that the changes induced by processes related to ta-C deposition, such as C subplantation or

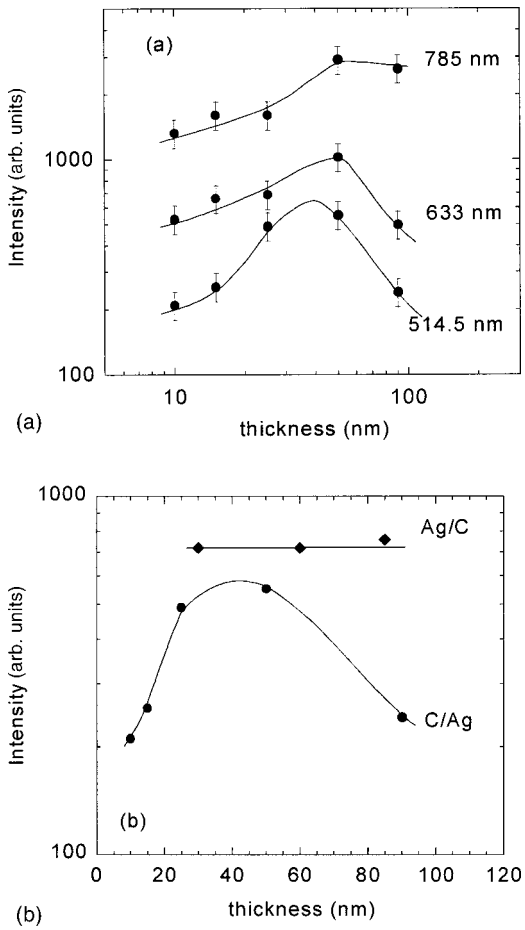

FIG. 7. (a) SERS intensity I as a function of thickness, for different excitation wavelengths and for Ag clusters produced in a He atmosphere. Increasing the excitation wavelength tunes the SERS effect into resonance. (b) Comparison between situations when Ag is on top or underneath the ta-C layer. Green wavelength (514.5 nm) was used in this case.

diffusion into Ag, appear to be similar to those induced in the carbon subsurface by Ag evaporation.

V. DISCUSSION

A. Factors controlling the SERS effect

In Sec. IV, a complex picture emerged about how the SERS effect depends on the type of Ag clusters, carbon film thickness and structure, and excitation wavelength. When the carbon film is an overlayer, its thickness affects the SERS effect through the dielectric properties of the overlayer, causing resonance effects. On the other hand, because the carbon film thickness is comparable with the probe wavelength, interference can affect both the SERS and the normal Raman signal. Interference Raman scattering has been shown to selectively probe either the surface, the interface, or the bulk,[37] while by placing the film in between thin layers of appropriately chosen materials, the signal of interest was also enhanced.[62]

1. Tuning into the SERS resonance

To discuss these aspects, we considered the simple model of an Ag spherical particle coated with a ta-C layer of thickness t, and then placed in air. The quasistatic (Rayleigh) formalism was used since it is the simplest to manipulate. This is not strictly applicable to our Ag nanostructures, because of their dimensions and dense packing. However, one can still reach valuable conclusions about how the dielectric functions of Ag and carbon overlayer determine the characteristics of the plasmon resonance. These trends tend to remain the same regardless the formalism used, static or electrodynamic, as indicated by calculations for embedding media with simple dielectric properties, such as water.[39]

The choice of the dielectric functions for Ag and ta-C require some discussion. In a rigorous treatment, one should take into account the mixed, more sp^2-rich, interface region, for which one should consider a spatially varying dielectric constant. However, in order to keep the calculations simple while still capturing the essential dependencies, we first considered the dielectric function of the carbon overlayer equal to that of bulk ta-C [Figs. 10(a) and 10(b)], and then observed how the enhancement values and resonance positions are affected by considering an interfacial layer with the dielectric function of a more sp^2 rich carbon, of lower density [Fig. 10(c)].

$\mathrm{Re}(\varepsilon)=\varepsilon_1$ and $\mathrm{Im}(\varepsilon)=\varepsilon_2$ of ta-C (Fig. 8) were obtained from a Kramers-Kronig analysis performed on low-energy EELS spectra,[63] and corroborated with values from spectroscopic ellipsometry.[64] ε_2 is nearly zero below 1.2 eV, and increases moving toward the UV, while ε_1 is high ($\sim$6–7) over the whole visible range. For $\mathrm{Re}(\varepsilon_m)=\varepsilon_{m1}$ and $\mathrm{Im}(\varepsilon_m)=\varepsilon_{m2}$ of Ag, we used the bulk values from Ref. 65. This is strictly justified only for features above about 100 nm, below which surface scattering limits the electron mean free path.[40] ε has two origins: interband electron transitions and Drude losses related to the relaxation time of the electrons in the plasmon, which increase due to surface scattering. The most affected is ε_{m2} which increases as $\varepsilon_{m2}=\varepsilon_{m2,\mathrm{interband}}+(3/4)\times(\omega_b^2/\omega^3)(\nu_F/a)$. Here ω_b is the Ag bulk plasmon frequency (corresponding to an energy of 9 eV), $\nu_F=1.4\times10^8$ cm/s is the Fermi velocity for Ag, ω is the incident frequency, and a is the Ag nanoparticle size. To give an order of magnitude, this correction increases ε_{m2} by a factor less than 2 for excitation energies decreasing from 2.8 to 1.6 eV in the case of 10-nm sized of Rayleigh Ag particles. From Fig. 8 we note also that ε_2 and ε_{m2} have inverse tendencies, increasing and decreasing, respectively, with increasing energy.

Both real and imaginary parts of Ag and ta-C are important for the spectral position and magnitude of the plasmon resonance. Their effects are shown in Fig. 1(a), which was derived using relations (1), (2), and (5), and the assumption that ta-C is an infinitely thick embedding layer. The high value of ε_1 ($\sim$7) causes an important shift of ω_{pl}, from near UV ($\omega_0=3.4$ eV), when air is the embedding environment, to red ($\omega_\infty=2$ eV). This shift is accompanied by an increase of the maximum of the resonance [Fig. 1(a)]. On the other hand, the nonzero values of ε_2 and ε_{m2} ($\sim$ 0.6 and 1 in red, respectively) damp and broaden the resonance.

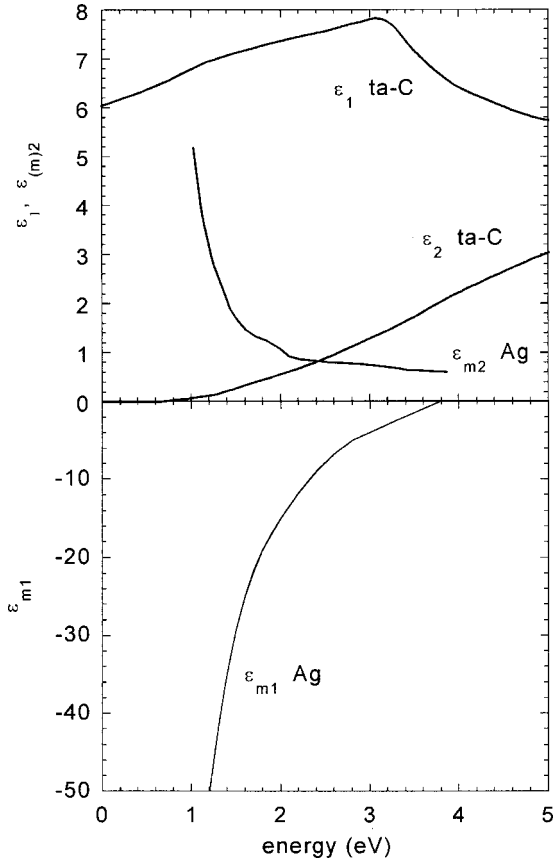

FIG. 8. Dielectric functions for Ag and bulk ta-C.

The ω_{pl} shift from near UV to red occurs gradually with increasing thickness t of the ta-C overlayer, saturating for the highest thicknesses, and Fig. 9 shows $G=|E|^4/|E_0|^4$ calculated at the ta-C side of the Ag/ta-C interface. The electric field decays in ta-C according to relation (5). The behavior

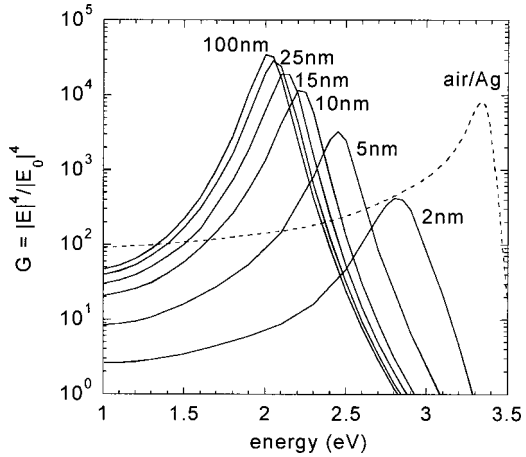

FIG. 9. Plasmon resonance redshift as a function of the ta-C overlayer thickness calculated using the quasistatic model; ω_{pl} shifts from $\omega_0=3.4$ eV when there is no ta-C overlayer (dashed line), to $\omega_\infty=2$ eV when the ta-C overlayer becomes very thick. Note that, compared to Ag spheres in air, several nanometers of ta-C decrease the enhancement. A higher thickness is required to rise the enhancement above the values in air.

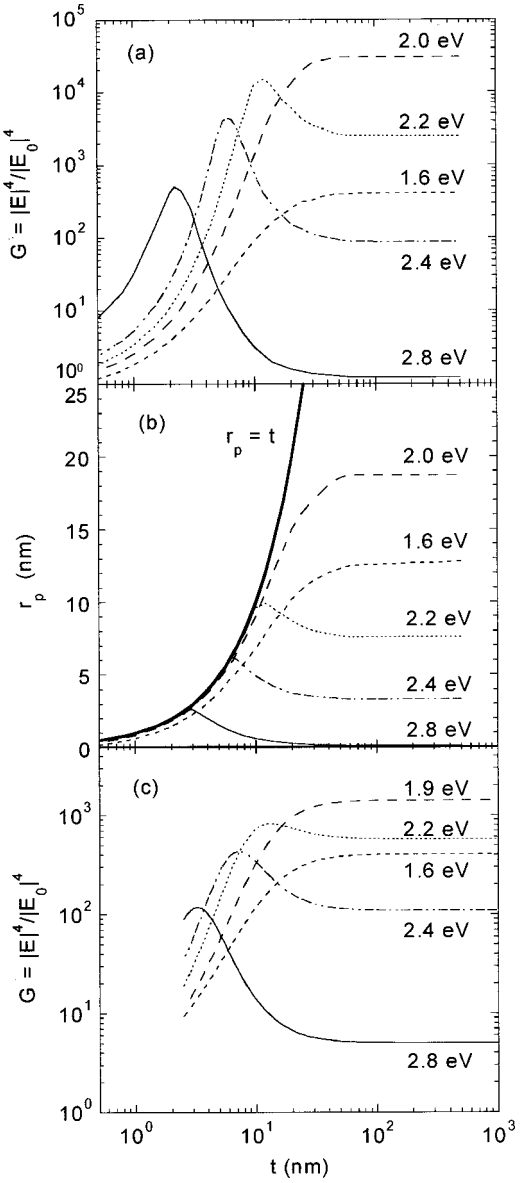

FIG. 10. Enhancement vs thickness for a 10-nm Ag sphere covered (a) by a layer of thickness t with the dielectric function of bulk ta-C, and (c) by 3 nm of sp^2-rich amorphous carbon (dielectric function from Ref. 67), followed by a layer of thickness t of bulk ta-C. (b) Range of the electric field associated with the plasmon excitation vs thickness at various excitation energies, calculated using the quasistatic model and the configuration from (a).

shown in Fig. 9 has important consequences for the spectral dependence of the relationship between G and t. One can qualitatively distinguish three cases, depending on the position of the excitation frequency ω_{ex} relative to ω_0 and ω_∞: (i) when $\omega_{\mathrm{ex}}\geqslant\omega_0$, G decreases with increasing t, saturating at low G values for large t; (ii) when $\omega_\infty<\omega_{\mathrm{ex}}<\omega_0$, G increases first with t, reaching a maximum for an intermediate t value, to further decrease at higher t values; and (iii) for $\omega_{\mathrm{ex}}\leqslant\omega_\infty$, G increases with increasing t, to saturate at high G values for large t.

Figure 10(a) shows calculated (G-t) dependencies for various ω_{ex}. The qualitative behaviors described above are

retrieved. Moreover, one can see that there is a ''spectral window'' for ω_{ex}, outside which the maximum enhancement begins to fall rapidly; here this is about 1.6–2.4 eV. This is due to ε_2 and ε_{m2} increasing significantly at each side of the spectral window (see Fig. 8). The surface scattering correction to ε_{m2} described above affects the enhancement at resonance shown in Fig. 10(a) by less than 10%. The electric-field range r_p, as defined in Sec. II, was also calculated, and found to follow almost the same dependence on t as G at the Ag/ta-C interface [Fig. 10(b)]. Therefore, the SERS intensity I obtained by integration according to Relation (6) will do the same, and this accounts for the shape of the experimental (I-t) dependencies from Fig. 7(a) for situations when $\omega_\infty < \omega_{ex} < \omega_0$ and $\omega_{ex} \leqslant \omega_\infty$. Note that Figs. 7(a) and 10(a) should be compared only qualitatively. In Fig. 7(a) the overall variation across the thickness range is much less pronounced than in the simulations, while the maximum position also shifts less. This can be explained by broadening and red-shifting of the theoretical resonances from Fig. 10(a) due to larger-size particles and electromagnetic coupling in the actual Ag nanostructures, as discussed in Sec. II.

Figure 10(b) shows, as a function of t and ω_{ex}, what fraction of t, r_p/t, is probed by SERS. The line $r_p = t$ indicates the limit case when the SERS signal would originate from the entire thickness t, while departing from it indicates that a decreasingly small fraction contributes. Also note that even for regions in the plasmon electric field range r_p, the contribution to SERS is uneven as the electric field decays rapidly as $(a/r)^{12}$.[66] This also means that by increasing the particle size a, one can increase the range of the plasmon effect. Figure 10(b) exemplifies how appropriate choices of t and ω_{ex} can be used to selectively probe different film regions. For $t \geqslant 100$ nm, only a fraction of t is probed even in the most favorable case (about 20% at $\omega_{ex} = 1.8$ eV). Increasing t and decreasing ω_{ex} strongly reduces r_p/t. On the other hand, for small t ($10 < t < 30$ nm), a much higher percentage, about 40–100%, is probed at all ω_{ex} values; while for very small t (<10 nm) the whole layer can be probed at high ω_{ex}. Moreover, for each t there is a resonant ω_{ex} at which r_p/t is maximum. The reduced SERS range compared with the film thickness for larger t values confines the active layer near the ta-C substrate interface, so that there is only little thickness dependence of the enhanced intensity I through r_p, in contrast with the nonenhanced intensity I_0 which is obtained in equal measure from the whole ta-C layer. This confirms that the experimental decay of I/I_0 with t from Figs. 5 and 6 occurs from I_0, as explained in Sec. IV.

The thickness independence of I with t for thicker films with Ag nanostructures on top [Fig. 7(b)] can now be understood. Now the embedding medium is air, so that there is no reason for ω_{pl} to redshift with decreasing the ta-C underlayer thickness. Therefore, for a rough surface like in Fig. 1(b), ω_{pl} should be in the 2.8–3-eV range. Moreover, the constancy of I with decreasing t down to about 20–30 nm is in agreement with the range r_p calculated above.

The values reported above in Fig. 10(a), obtained by using the optical constants of bulk ta-C are modified by the presence at the interface with Ag of a few nanometers of a more sp^2 rich material (as mentioned in Secs. III and IV).

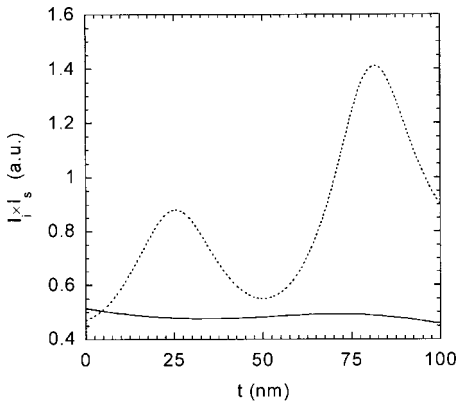

FIG. 11. Interference modulation function $I_i \times I_s$ for specular Ag surfaces (dashed line), and a rough Ag surface with the roughness derived from Fig. 2(b). Calculations were performed for the 514.5-nm excitation.

Figure 10(c) shows the results of the quasistatic simulation for the four-layer system describing this situation: an Ag sphere (10-nm diameter)/3 nm of sp^2-rich amorphous carbon, of density 2.2 g/cm^3/bulk ta-C/air. The 3-nm sp^2-rich interfacial layer makes the maximum enhancement G decrease moderately when compared to Fig. 10(a), by about one order of magnitude at a given wavelength, and slightly shifts the resonance position from 2 to 1.9 eV.

2. Interference

To assess any effects due to interference which might affect the data from Fig. 7, the system was modeled as a four-layer structure of, in order, vacuum/ta-C/Ag/Si. Using standard techniques for determining reflection and transmission coefficients for multilayer structures from the Fresnel coefficients for individual interfaces, the light intensity incident at the ta-C/Ag interface I_i was evaluated as a function of the ta-C overlayer thickness. Similarly, the effects of interference on the Raman-scattered light were assessed by considering the scattered light generated at the ta-C/Ag interface I_s and directed normal to it. The product of these two functions $I_i \times I_s$ approximates the modulation of the intensity of the SERS signal with the thickness of the ta-C film. The G-t dependence of the scattered light due to tuning into the plasmon resonance (as described above in Sec. V A 1) was neglected, in order to separate the effect of interference. The modulation $I_i \times I_s$ is quite important in the case of flat (specular) Ag films (Fig. 11). The interfacial roughness caused by the clustered nature of the Ag films strongly reduces it, and this was modeled by correcting the Fresnel reflection coefficients using the method of Stearns.[68] One can thus conclude that the G-t dependencies from Fig. 7 are indeed due to tuning in and out of resonance by varying the overlayer's thickness.

How do our experimental enhancement values compare with the estimations above? $R = I/I_0$ has a strong thickness dependence [see relation (7)], while the quantity $(t \times R)$ eliminates it, giving the enhancement factor integrated over the film thickness. Our experimental data (Fig. 6) give $(t \times R)$ values between 10^4 and 10^5 over the whole thickness

range at 785-nm excitation. These values are above those obtained in Fig. 10(c), when the sp^2-rich interfacial layer was taken into account. This indicates that resonance coupling between closely packed particles, like the 20-nm structures from Fig. 2(b), might take place. Indeed, from electrodynamic simulations for of rough surface formed by packed semispherical particles of 30 nm,[41] an optimal packing of the particles [i.e., $d=2r$ in Fig. 1(b)] would give averaged enhancement factors up to 10^6, while if the packing is slightly nonoptimal ($d>2r$), the enhancement falls to below 10^4. For the random films from Fig. 2(a) it is possible that ''hot spots'' are responsible for the enhancement. Nevertheless, from our measurements with a micron size beam there is no direct evidence to support this fact, as in Ref. 59, as the site to site fluctuations recorded here reached only a factor of about 5.

B. Enhancement contrast and material identification

Figure 1(a) shows that $\mathrm{Im}(\varepsilon)=\varepsilon_2$ of the overlayer causes damping of the resonance. Consequently, SERS works better on carbon materials with low ε_2 in the visible range such as ta-C. C_{60} and fullerite are other good cases, as ε_2 is nearly zero for energies below 2 eV.[69] At the other extreme, there is graphite, whose ε_2 values in visible reach 8–9. This makes graphite inactive for SERS. Other materials, like amorphous carbons deposited in various conditions have ε_2 values lying in between these two extremes.[70,71] One can pass from amorphous carbon to nanocrystalline graphite in a continuous transition, either using thermal annealing, or high-energy particle irradiation. In such a transition, the amorphous network undergoes several transformations: (i) there is sp^3 to sp^2 conversion, and (ii) clustering of the sp^2 phase into more stable aromatic rings.[15,16] By increasing the annealing temperature or the irradiation dose, sp^2 clusters of increasing size form in the amorphous sp^3 matrix, until this disappears and the material transforms into nanocrystalline graphite. The graphitization induced by irradiation can affect the SERS effect in three ways.

(i) The clustering of the sp^2 phase into aromatic rings affects the shape of the Raman spectrum, through the *D* peak around 1360 cm^{-1}.[15,16,55] With an increasing size of aromatic clusters, the *D* peak increases relative to the *G* peak, so that the Raman parameter $I(D)/I(G)$ increases. The Raman intensity also increases with sp^3 to sp^2 conversion as the sp^2 phase has a higher cross section than the sp^3 phase (see Sec. IV).

(ii) In the transition toward nanocrystalline graphite, an anisotropy of the polarizability occurs as the sp^2 aromatic clusters tend to orient in preferential planes, so that the maximum polarizability is in the plane of the aromatic clusters. During post-deposition thermal annealing the sp^2 aromatic clusters tend to orient in planes parallel to the substrate,[72] while high-energy particle irradiation aligns them perpendicular to the substrate.[73] Therefore the coupling with the electromagnetic field in SERS can be maximized if the direction of the incident electric field is in the plane of the sp^2 aromatic clusters. The effect of the polarizability orientation, when perpendicular or parallel to the electric field, has been demonstrated in experiments using polyimide molecules.[74]

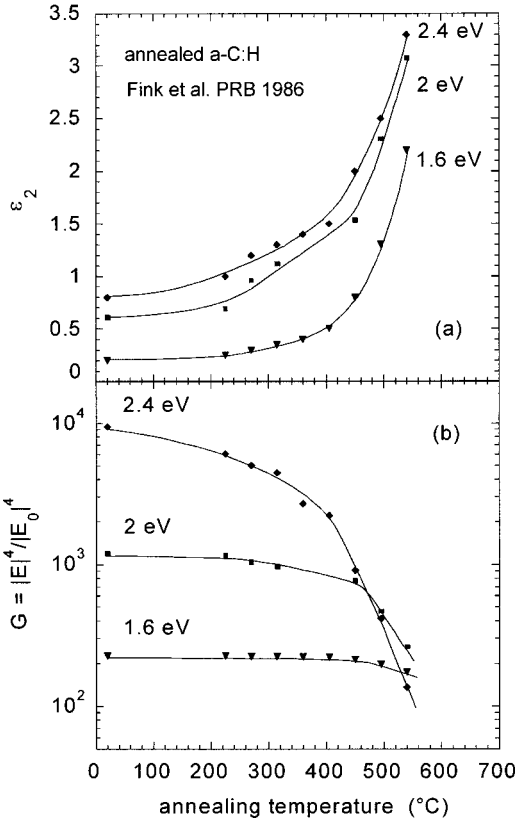

FIG. 12. (a) Change in the imaginary part of the dielectric constant of *a*-C:H during its graphitization process through thermal annealing. Data are taken from Ref. 70. (b) Corresponding changes in the SERS enhancement reflecting the sensitivity of the SERS effect to the dielectric function.

(iii) The dielectric function changes sensibly during the graphitization process: $\mathrm{Im}(\varepsilon)$ increases strongly toward the graphite values (~8–12), while $\mathrm{Re}(\varepsilon)$ changes only slightly.[70] As an example, Fig. 12(a) shows the evolution of $\mathrm{Im}(\varepsilon)$ of thermally annealed *a*-C:H with the annealing temperature. ε was obtained in this case by a Kramers-Kronig analysis performed on the low energy EELS spectra.[70] The increase in $\mathrm{Im}(\varepsilon)$ makes the SERS enhancement *G* eventually drop to zero [Fig. 12(b)]. *G* varies significantly at plasmon resonance, which in the quasistatic model is displaced to 2.4 eV due to the lower ε_1 of *a*-C:H's (~4) compared to that of ta-C (~6–7).

The graphitization induced by irradiation will, consequently, manifest itself through two signatures in SERS: the shape of the Raman signal changes to reflect clustering of the sp^2 phase, and, second, the SERS enhancement at resonance eventually decreases due to the high increase of the imaginary part of the dielectric constant. As the dielectric function is very sensitive even to small variations in film structure [see Fig. 11(a)], which might not be reflected by changes in the Raman spectra, one can follow the transition from ta-C to graphite entirely by monitoring the decrease of the intensity *I* toward I_0.

VI. CONCLUSION

We investigated the possibility of achieving nanometer-scale sensitivity in a surface enhanced Raman experiment while using larger-sized probes of 0.1–1 μm. Carbon overlayers cover Ag nanostructures so that regions close to the film-substrate interface are probed, this geometry complementing the surface sensitive scanning near-field techniques. The main application targeted was carbon film transformation under *e*-beam irradiation, and here we discussed, as an example, the transformation of tetrahedral amorphous carbon (ta-C) into nanocrystalline graphite. The SERS effect with ta-C as the overlayer was found to depend on the Ag nanostructure size, overlayer thickness, and excitation wavelength. Enhancement factors, averaged over the film thickness and a μm^2 size area, of about 10^3-10^4 were obtained for several tens of nm thick ta-C overlayers at resonance, in the nearinfrared. Modulations of the enhancement with the overlayer thickness were attributed to tuning in and out of the SERS resonance, while interference effects were highly reduced due to the rough nature of the Ag films. The SERS effect is highly sensitive to the more sp^2-rich interfacial layer of ta-C, though it also extends into the film's bulk. This sensitivity is increased by a selective enhancement of the Raman *D* band, attributed to an increased coupling caused by the alignment of the direction of maximum polarizability to the incident electric field. The change of the overlayer dielectric function upon irradiation can be used to produce an enhancement contrast, and allows a material identification. This contrast based technique could be extended to other non-carbon materials and to local mapping of dielectric properties of materials.

ACKNOWLEDGMENTS

The authors wish to thank Dr. D. R. Richards for many useful comments, and Professor T. W. Clyne and D. Roy for help with the Raman facilities. A.I. gratefully acknowledges a Research Fellowship from Girton College, Cambridge.

*Corresponding author. Email address: ai205@eng.cam.ac.uk

[1] A. A. Talin, L. S. Pan, K. F. McCarty, T. E. Felter, H. J. Doerr, and R. F. Bunshah, Appl. Phys. Lett. **69**, 3842 (1996).

[2] B. F. Coll, J. E. Jaskie, J. L. Markham, E. P. Menu, A. A. Talin, and P. von Allmen, in *Covalently Bonded Disordered Thin-Film Materials*, edited by M. P. Siegal, J. G. Jaskie, and W. Milens, MRS Symposia Proceedings, No. 498 (Materials Research Society Pittsburgh, PA, 1998), p. 185.

[3] A. N. Obralsov, I. Yu. Pavlovsky, A. P. Volkov, J. Vac. Sci. Technol. B **17**, 674 (1999).

[4] G. A. J. Amaratunga, M. Baxendale, N. Rupesinghe, I. Alenxandrou, M. Chhowala, T. Butler, A. Munindradasa, C. J. Kiely, L. Zhang, and T. Sakai, New Diamond Front. Carbon Technol. **9**, 31 (1999).

[5] B. S. Satyanarayana, J. Robertson, and W. I. Milne, J. Appl. Phys. **87**, 3126 (2000).

[6] A. Ilie, A. C. Ferrari, T. Yagi, S. E. Rodil, and J. Robertson, J. Appl. Phys. **90**, 2024 (2001).

[7] D. R. McKenzie, W. T. Li, E. G. Gerstner, A. Merchant, D. G. McCulloch, N. A. Marks, and M. M. Bilek, Diamond Relat. Mater. **10**, 230 (2001).

[8] D. G. McCulloch, E. G. Gerstner, D. R. McKenzie, S. Prawer, and R. Kalish, Phys. Rev. B **52**, 850 (1995); M. Waiblinger, Ch. Sommerhalter, B. Pietzak, J. Krauser, B. Mertsacker, M. Ch. Lux-Steiner, S. Klaumunzer, A. Weidinger, C. Ronning, and H. Hofsass, Appl. Phys. A: Mater. Sci. Process. **69**, 239 (1999).

[9] D. Ugarte, Nature (London) **359**, 707 (1992); T. Cabioc'h, J. P. Riviere, and J. Delafond, J. Mater. Sci. **30**, 4787 (1995).

[10] F. Banhart and P. M. Ajayan, Nature (London) **382**, 433 (1996).

[11] C. A. Davis, D. R. McKenzie, Y. Yin, E. Kravtchinskaia, G. A. J. Amaratunga, and V. S. Veerasamy, Philos. Mag. B **69**, 1133 (1994).

[12] C. A. Davis, G. A. J. Amaratunga, and K. M. Knowles, Phys. Rev. Lett. **80**, 3280 (1998).

[13] F. Tuinstra and J. L. Koening, J. Chem. Phys. **53**, 1126 (1970).

[14] R. J. Nemanich and S. A. Solin, Phys. Rev. B **20**, 392 (1979).

[15] R. O. Dillon, J. A. Woollam, and V. Karkanant, Phys. Rev. B **29**, 3482 (1984); M. A. Tamor and W. C. Vassel, J. Appl. Phys. **76**, 3823 (1994).

[16] A. C. Ferrari and J. Robertson, Phys. Rev. B **61**, 14 095 (2000).

[17] A. M. Rao, F. Richter, S. Bandow, B. Chase, P. C. Eklund, K. A. Williams, S. Fang, K. R. Subbaswamy, M. Menon, A. Thess, R. E. Smalley, G. Dresselhaus, and M. S. Dresselhaus, Science **275**, 187 (1997).

[18] R. J. Nemanich, Annu. Rev. Mater. Sci. **21**, 535 (1991); S. Prawer and K. W. Nugent, in *Amorphous Carbon: State of the Art*, edited by S. R. P. Silva, J. Robertson, W. I. Milne, and G. A. J. Amaratunga (World Scientific, Singapore, 1998).

[19] G. S. Duesberg, J. Muster, M. Burghard, H. J. Byrne, and S. Roth, AIP Conf. Proc. **486**, 338 (1999); K. Kneipp, H. Kneipp, P. Corio, S. D. M. Brown, K. Shafer, J. Motz, L. T. Perelman, E. B. Hanlon, A. Marucci, G. Dresselhaus, and M. S. Dresselhaus, Phys. Rev. Lett. **84**, 3470 (2000).

[20] P. Hildebrandt and M. Stockburger, J. Phys. Chem. **88**, 5935 (1984); J. T. Golab, J. R. Sprague, K. T. Carron, G. C. Schatz, and R. P. van Duyne, J. Chem. Phys. **88**, 7942 (1988); K. Kneipp, Y. Wang, H. Kneipp, I. Itzkan, R. R. Dasari, and M. S. Feld, Phys. Rev. Lett. **76**, 2444 (1996).

[21] S. Nie and S. R. Emory, Science **275**, 1102 (1997).

[22] M. Moskovits and D. DiLella, in *Surface Enhanced Raman Scattering*, edited by R. K. Chang and T. E. Furtak (Plenum, New York, 1982), p. 243.

[23] T. Lopez-Rios, Diamond Relat. Mater. **5**, 608 (1996).

[24] D. S. Knight, R. Weimer, L. Pilione, and W. B. White, Appl. Phys. Lett. **56**, 1320 (1990).

[25] D. A. Smith, S. Webster, M. Ayad, S. D. Evans, D. Fogherty, and D. Batchelder, Ultramicroscopy **61**, 247 (1995).

[26] V. Deckerr, D. Zeisel, R. Zenobi, and T. Vo-Dinh, Anal. Chem. **70**, 2646 (1998).

[27] R. Stoeckle, Y. D. Suh, V. Deckert, and R. Zenobi, Chem. Phys. Lett. **318**, 131 (2000).

[28] P. J. Fallon, V. S. Veerasamy, C. A. Davis, J. Robertson, G. A. J. Amaratunga, W. I. Milne, and J. Koskinen, Phys. Rev. B **48**, 4777 (1993).

[29] M. Moskovits, Rev. Mod. Phys. **57**, 783 (1985).
[30] J. P. Kottmann, O. J. F. Martin, D. R. Smith, and S. Schultz, Phys. Rev. B **64**, 235402 (2001).
[31] V. M. Shalaev and A. K. Sarychev, Phys. Rev. B **57**, 13 265 (1998).
[32] F. Brouers, S. Blacher, A. N. Lagarkov, A. K. Sarychev, P. Gadenne, and V. M. Shalaev, Phys. Rev. B **55**, 13 234 (1997).
[33] V. A. Markel, V. M. Shalaev, P. Zhang, W. Huynh, L. Tay, T. L. Haslett, and M. Moskovits, Phys. Rev. B **59**, 10 903 (1999).
[34] A. Downes, M. E. Taylor, and M. E. Welland, Phys. Rev. B **57**, 6706 (1998).
[35] K. B. K. Teo, S. E. Rodil, J. T. H. Tsai, A. C. Ferrari, J. Robertson, and W. I. Milne, J. Appl. Phys. **89**, 3706 (2001).
[36] M. Ramsteiner, C. Wild, and J. Wagner, Appl. Opt. **28**, 4017 (1989).
[37] L. Yu. Khriachtchev, R. Lappalainen, and M. Rasanen, Diamond Relat. Mater. **7**, 1451 (1998).
[38] O. Stenzel, A. Stendal, D. Drews, T. Werninghaus, M. Falke, D. R. T. Zahn, and C. von Borczyskowski, Appl. Surf. Sci. **108**, 71 (1997).
[39] P. W. Barber, R. K. Chang, and H. Massoudi, Phys. Rev. B **27**, 7251 (1983).
[40] J. A. A. J. Perenboom and P. Wyder, Phys. Rep. **78**, 173 (1981).
[41] F. J. Garcia-Vidal and J. B. Pendry, Phys. Rev. Lett. **77**, 1163 (1996).
[42] P. Milani and S. Iannotta, *Cluster Beam Synthesis of Nanostructured Materials*, Springer Series in Cluster Physics (Springer, Berlin, 1999).
[43] X. Shi, B. G. Tay, and S. P. Lau, Int. J. Mod. Phys. B **14**, 136 (2000).
[44] A. LiBassi, A. C. Ferrari, V. Stolojan, B. K. Tanner, J. Robertson, and L. M. Brown, Diamond Relat. Mater. **9**, 771 (2000).
[45] A. Ilie, A. Hart, A. J. Flewitt, J. Robertson, and W. I. Milne, J. Appl. Phys. **88**, 6002 (2000).
[46] P. D. Maguire, D. P. Magill, A. A. Ogwu, and J. A. McLaughlin, Diamond Relat. Mater. **10**, 216 (2001); C. Srividya and S. V. Babu, Chem. Mater. **8**, 2528 (1996); D. P. Butt, K. C. Walter, M. Nastasi, A. L. Campuzano, P. S. Martin, B. P. Wood, D. J. Rej, and G. G. Miller, Philos. Mag. Lett. **70**, 385 (1994); C. Sella, J. Lecoeur, Y. Sampeur, and P. Catania, Surf. Coat. Technol. **60**, 577 (1993).
[47] N. Wada and S. A. Solin, Physica B & C **105**, 353 (1980); S. R. Salis, D. J. Gardiner, M. Bowden, J. Savage, and D. Rodvany, Diamond Relat. Mater. **5**, 589 (1996).
[48] C. A. Coulson and H. C. Longuet-Higgins, Proc. R. Soc. London, Ser. A **191**, 447 (1947); D. Beeman and R. Alben, Adv. Phys. **26**, 339 (1977).
[49] R. P. Vidano, D. B. Fischbach, L. J. Willis, and T. M. Loehr, Solid State Commun. **39**, 341 (1981).
[50] M. Ramsteiner and J. Wagner, Appl. Phys. Lett. **51**, 1355 (1987); I. Pocsik, M. Koos, M. Hundhausen, and L. Ley, in *Amorphous Carbon: State of the Art*, edited by S. R. P. Silva, J. Robertson, W. I. Milne, and G. A. J. Amaratunga (World Scientific, Singapore, 1998), p. 224.
[51] A. C. Ferrari and J. Robertson, Phys. Rev. B **64**, 075414 (2001).
[52] R. J. Nemanich, S. A. Solin, and R. M. Martin, Phys. Rev. B **23**, 6348 (1981).
[53] J. S. Lannin, J. Non-Cryst. Solids **97**, 39 (1987).
[54] S. Prawer, K. W. Nugent, Y. Lifshitz, G. D. Lempert, E. Grossman, J. Kulik, I. Avigal, and R. Kalish, Diamond Relat. Mater. **5**, 433 (1996).
[55] J. Robertson, Prog. Solid State Chem. **21**, 199 (1991).
[56] C. Thomsen and S. Reich, Phys. Rev. B **85**, 5214 (2000).
[57] I. Pocsik, M. Hundhausen, M. Koos, and L. Ley, J. Non-Cryst. Solids **227**, 1083 (1998).
[58] M. B. Tzolov, N. V. Tzenov, D. I. Dimova-Malinovska, and D. Y. Yankov, Appl. Phys. Lett. **62**, 2396 (1993).
[59] A. Kudelski and B. Pettinger, Chem. Phys. Lett. **321**, 356 (2000).
[60] J. C. Tsang, J. E. Demuth, P. N. Sanda, and J. R. Kirtley, Chem. Phys. Lett. **76**, 54 (1980).
[61] J. Robertson and R. P. O'Reilly, Phys. Rev. B **35**, 2946 (1987).
[62] R. J. Nemanich, C. C. Tsai, and G. A. N. Connell, Phys. Rev. Lett. **44**, 273 (1980); R. J. Nemanich, C. C. Tsai, M. J. Thompson, and T. W. Sigmon, J. Vac. Sci. Technol. **19**, 685 (1981).
[63] S. Waidmann, M. Knupfer, J. Fink, B. Kleinsorge, and J. Robertson, Diamond Relat. Mater. **9**, 722 (2000).
[64] Z. Y. Chen and J. P. Zhao, J. Appl. Phys. **87**, 4268 (2000).
[65] W. D. Lynch and W. R. Hunter, in *Handbook of Optical Constants of Solids*, edited by E. D. Palik, (Academic, New York, 1985).
[66] S. L. McCall, P. M. Platzmann, and P. A. Wolff, Phys. Lett. **77A**, 381 (1980); M. Kerker, D. S. Wang, and H. Chew, Appl. Opt. **19**, 3373 (1980).
[67] *Handbook of Optical Constants of Solids*, edited by E. D. Palik, (Academic, New York, 1985).
[68] D. G. Steams, J. Appl. Phys. **65**, 491 (1989).
[69] S. L. Ren, Y. Wang, A. M. Rao, E. McRae, J. M. Holden, T. Hager, K. Wang, W.-T. Lee, W. F. Ni, J. Selegue, and P. C. Eklund, Appl. Phys. Lett. **59**, 2678 (1991); G. Guizzetti, F. Marabelli, M. Patrini, V. Capozzi, G. F. Lorusso, A. Minafra, M. Manfredini, and P. Milani, Phys. Status Solidi B **183**, 267 (1994).
[70] J. Fink, Th. Mueller-Heinzerling, J. Pflueger, and B. Scheerer, B. Dischler, P. Koidl, A. Bubenzer, and R. E. Sah, Phys. Rev. B **30**, 4713 (1984).
[71] Y. Lifshitz, G. D. Lempert, E. Grossman, H. J. Scheibe, S. Voellmar, B. Schultrich, A. Breskin, R. Chechik, E. Shefer, D. Bacon, R. Kalish, and A. Hoffman, Diamond Relat. Mater. **6**, 687 (1997).
[72] J. P. Sullivan, T. A. Friedmann, and A. G. Baca, J. Electron. Mater. **26**, 1021 (1997).
[73] S. S. Kim, S. Hishita, T. S. Cho, and J. H. Je, J. Appl. Phys. **88**, 55 (2000).
[74] W. H. Tsai, J. T. Young, F. J. Boerio, and P. P. Hong, Langmuir **7**, 745 (1991).